Available online at www.sciencedirect.com
SCIENCE DIRECT
Journal of Colloid and Interface Science 279 (2004) 186–191
JOURNAL OF Colloid and Interface Science
www.elsevier.com/locate/jcis

The maximum contact angle at the rim of a heavy floating disk

Todd I. Hesla, Daniel D. Joseph *

Department of Aerospace Engineering and Mechanics, University of Minnesota, Minneapolis MN, USA

Received 21 October 2003; accepted 16 June 2004

Available online 21 July 2004

Abstract

We give a simple mathematical argument that as the weight of a floating disk is gradually increased, the maximum contact angle at its sharp rim which is attained before the disk sinks is greater than 90°, and present numerical results which support this conclusion.

Keywords: Contact angle; Surface tension; Sharp edge; Floating

1. Introduction

We consider the equilibrium of a circular disk of radius a, height h, and uniform density ρ_s, held by surface tension at the surface of a quiescent liquid of density ρ (see Fig. 1). We shall assume that $\rho_s > \rho$. In order to make the problem axisymmetric, we shall further assume that (at equilibrium) the disk axis is vertical, and that either the liquid extends to infinity in all horizontal directions or that it is bounded by a cylindrical wall, coaxial with the disk, of finite radius $A > a$. Under these assumptions, we may assume that the entire liquid surface is axisymmetric about the disk axis.

The contact line between the liquid and solid surfaces will tend to remain attached to the sharp upper rim of the disk, and the contact angle α_0 will adjust itself until the total upward force on the disk equals its weight $W = \pi a^2 h \rho_s g$. According to Princen [1, p. 34] this will happen as long as α_0 remains less than the advancing contact angle. In the remainder of the discussion we will assume this to be the case.

If ρ_s (and thus W) is gradually increased, the disk will sink lower and lower until at some point the surface can no longer support it; it then breaks free and sinks to the bottom. We are interested in the value of α_0 at the moment when ρ_s reaches this maximum value. We will see that this maximum value of α_0 is strictly greater than 90°, a result which is somewhat contrary to intuitive expectation.

In the related *two*-dimensional problem of a floating rectangle of half-width a and height h, the equations can be integrated analytically. The case $h = 2a$ is discussed by Princen [1, pp. 34–36], although his objective—to determine the maximum value of a for a given value of ρ_s—is in a sense the opposite of ours. His results are therefore not directly comparable to ours, although it is interesting to note that his Fig. 24, which is to some extent analogous to our Fig. 7, shows that the maximum value of α_0 exceeds 90° in two dimensions, also. He does not, however, make any mention of this fact in his discussion.

2. Qualitative discussion

The key to understanding the aforementioned "breakaway" scenario is the vertical force balance: W is balanced by the sum of the total pressure force F_{pres} on the disk and the surface tension force F_{surf} on its rim. Symbolically,

$$W = F_{\text{pres}} + F_{\text{surf}}. \tag{1}$$

(The net horizontal force is automatically 0 by axisymmetry; we therefore need only consider vertical forces.)

The equilibrium pressure p in the liquid is given by the law of hydrostatics. For convenience we assume that the pressure in the air above the liquid is everywhere 0, and we

* Corresponding author. Fax: +1-612-626-1558.
E-mail addresses: hesla@aem.umn.edu (T.I. Hesla), joseph@aem.umn.edu (D.D. Joseph).

0021-9797/$ – see front matter
doi:10.1016/j.jcis.2004.06.055

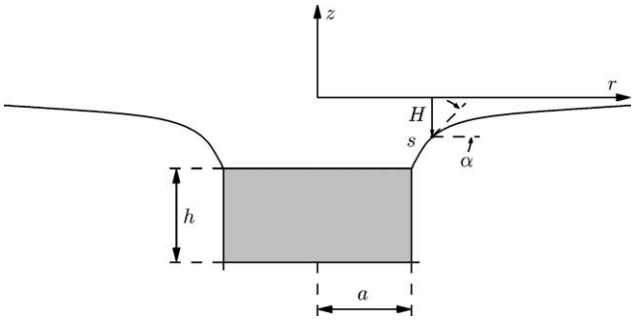

Fig. 1. Disk suspended by surface tension (side view).

choose the origin of the z axis to be the level where p also equals 0. (This is *not* the level of the upper surface of the disk. In fact, if $A = \infty$, it is the level of the liquid surface infinitely far from the disk, as suggested by Fig. 1.) If g is the acceleration of gravity, the law of hydrostatics then takes the form

$$p = -\rho g z. \tag{2}$$

Since the total pressure force on the upper surface of the disk is obviously 0 and the lateral surface of the disk is exactly vertical, we obtain

$$F_{\text{pres}} = \pi a^2 \rho g(-H_0 + h), \tag{3}$$

where H_0 is the z-coordinate of the upper surface of the disk. On the other hand, if γ is the surface tension (assumed constant), then

$$F_{\text{surf}} = 2\pi a \gamma \sin\alpha_0. \tag{4}$$

As W is gradually increased and the disk sinks lower (H_0 decreases), we expect that α_0 will gradually increase. Since F_{surf} is proportional to $\sin\alpha_0$, it also will increase—until α_0 reaches 90°. Once α_0 exceeds 90°, however, $\sin\alpha_0$—and therefore F_{surf}—begins to decrease again. Since presumably H_0 continues to decrease (and thus F_{pres} to increase), the obvious question is whether the sum of F_{surf} and F_{pres} will be increasing or decreasing.

The answer becomes clear when we compare the instantaneous rates of change of F_{surf} and F_{pres}. Note that at the moment when $\alpha_0 = 90°$, $\sin\alpha_0$—and thus F_{surf}—has rate of change 0. However, since H_0 presumably continues to decrease (and thus F_{pres} to increase) at a rate of order 1, the sum of F_{pres} and F_{surf} will continue to increase *for a while* after α_0 exceeds 90°. It follows that the maximum value of W which can be supported occurs when α_0 is somewhat greater than 90° (assuming that this angle is less than the advancing contact angle). This conclusion is borne out by the numerical results reported in Section 5.

3. Exact analysis

An exact analysis must take account of the coupling between W, H_0, α_0, and the shape of the surface. The latter is determined by the law of Laplace—the jump in pressure across the surface equals γ times twice the mean curvature. Since the pressure above the surface is here assumed to be 0 and that below is given by (2), the law of Laplace can be written

$$\gamma\left(\frac{1}{R_1} + \frac{1}{R_2}\right) = \rho g H, \tag{5}$$

where R_1 and R_2 are the principal radii of curvature of the surface (taken as positive if the corresponding centers of curvature lie above the surface) and H is the z-coordinate of the surface.

Since the problem is axisymmetric, the shape of the surface is completely determined by the curve $(r(s), H(s))$ along which the surface intersects a vertical plane through the disk axis, where r is the radial coordinate and s is the arc length along the curve, measured from the upper rim of the disk (see Fig. 1). If $\alpha(s)$ is the local inclination of this curve, defined as the unique angle satisfying

$$\cos\alpha(s) = r'(s), \quad \sin\alpha(s) = H'(s), \tag{6}$$

then (5) can be written

$$\alpha'(s) + \frac{H'(s)}{r(s)} = \frac{\rho g}{\gamma} H(s). \tag{7}$$

A second differential equation relating $r(s)$ and $H(s)$ is the condition

$$r'(s)^2 + H'(s)^2 = 1 \tag{8}$$

that s be arc length along the curve.

3.1. Boundary conditions

If we add appropriate boundary conditions at the initial (inner) and terminal (outer) points of the curve, Eqs. (7) and (8) (in conjunction with (6)) become a (nonlinear) two-point boundary-value problem for $r(s)$ and $H(s)$. Since (7) is essentially a second-order differential equation, it requires a boundary condition at each end. However, (8) is only of first order and thus requires a condition at only one end; for convenience we will use a condition at the inner end.

To facilitate numerical solution of the problem, we assume that the liquid is contained in a *finite* cylindrical tank (coaxial with the disk) of radius $A > a$; we shall comment briefly below about the infinite case. At the inner end of the curve we have $s = 0$. We do not, however, know the value of s at the outer end of the curve since the total length L of the curve is not known a priori. An additional equation must therefore be added to determine L and close the system. This equation will appear as an additional boundary condition at the outer end of the curve, bringing the total number of boundary conditions to four—two at the inner end and two at the outer.

3.1.1. Outer boundary conditions

At the tank wall the contact angle is fixed by the Young–Dupré law; this amounts to a specification of $H'(L)$. To simulate the infinite problem, we shall take $A \gg a$ and require that

$$H'(L) = 0 \tag{9}$$

(that is, that the contact angle be 90°). For the additional boundary condition mentioned above we shall use

$$r(L) = A. \tag{10}$$

If the liquid extends to infinity in all directions, we assume that

$$\lim_{s\to\infty} H'(s) = 0.$$

Alternatively, we could require that

$$\lim_{s\to\infty} r(s)H'(s) = 0.$$

Note that in this case the parameter interval, $[0,\infty)$, is *known*; consequently no additional boundary condition is required to close the system.

3.1.2. Inner boundary conditions

At the inner end of curve, we have

$$r(0) = a. \tag{11}$$

A second condition is provided by the vertical force balance (1). Inserting (3) and (4) and dividing by πa, this equation can be written

$$2\gamma H'(0) = a\rho g\left(H(0) + h\left(\frac{\rho_s}{\rho} - 1\right)\right). \tag{12}$$

3.2. Dimensionless form

Eqs. (7) and (8) (in conjunction with (6)), together with boundary conditions (9)–(12), comprise a formally complete system of equations for the two unknown functions $r(s)$ and $H(s)$ and the scalar unknown L.

For the numerical solution we shall use the dimensionless form of these equations. Using a as the characteristic length and denoting the dimensionless forms of s, r, and H by the same symbols, the equations become

$$\alpha'(s) + \frac{H'(s)}{r(s)} = \mathcal{B}H(s), \tag{13}$$

$$r'(s)^2 + H'(s)^2 = 1, \tag{14}$$

$$r(0) = 1, \tag{15}$$

$$2H'(0) = \mathcal{B}\big(H(0) + \mathcal{W}\big), \tag{16}$$

$$r(\mathcal{L}) = \mathcal{A}, \quad \text{and} \tag{17}$$

$$H'(\mathcal{L}) = 0, \tag{18}$$

where

$$\mathcal{B} = \frac{\rho g a^2}{\gamma}$$

is the Bond number,

$$\mathcal{W} = \frac{h}{a}\left(\frac{\rho_s}{\rho} - 1\right)$$

is the dimensionless buoyant weight (equal to the buoyant weight divided by $\pi a^3 \rho g$), and

$$\mathcal{L} = \frac{L}{a}, \quad \mathcal{A} = \frac{A}{a}.$$

(Eq. (6) is already dimensionless, so it does not change.)

The system of Eqs. (13)–(18) is a nonlinear two-point boundary-value problem. In the associated initial-value problem we would specify both $H(0) = H_0$ and $\alpha(0) = \alpha_0$, and impose *no* condition at $s = \mathcal{L}$. Since solutions of initial-value problems are unique, it follows that each solution of (13)–(18) is a is uniquely associated with the corresponding values of α_0 and H_0. The set of all solutions, therefore, is in one-to-one correspondence with a certain curve in the (α_0, H_0) plane, which we shall refer to as the *solution curve* (not to be confused with the curve $(r(s), H(s))$ in the (r, z) plane). Some numerically generated solution curves are shown in Figs. 2–6. In looking at these figures, it should be kept in mind that it is only the lowermost branch of each, for α_0 between 0° and 180°, which is of physical interest. Note that there are multiple solutions for some values of α_0 (or H_0).

4. Numerical scheme

In light of the discussion in Sections 1 and 2 we expect that the system (13)–(18) has a solution *only* if $\mathcal{W}$ does not exceed a certain maximum value. Our objective is to determine this maximum value, and the associated value of α_0. Since the system does not have an explicit solution, it must be solved numerically.

A finite-difference scheme can be constructed as follows. Let N be a fixed positive integer, and choose a partition

$$0 = s_0 < s_1 < \cdots < s_N = \mathcal{L}$$

of the parameter interval $[0, \mathcal{L}]$ into N subintervals. Corresponding to each partition point s_i, we introduce discrete approximations r_i and H_i of $r(s_i)$ and $H(s_i)$, respectively.

The most natural procedure is to use equal subintervals, each of length equal to the unknown quantity $\Delta s = \mathcal{L}/N$. There are then a total of $2N + 3$ unknowns to determine:

$$r_0, r_1, \ldots, r_N, \quad H_0, H_1, \ldots, H_N, \quad \text{and} \quad \Delta s.$$

In constructing finite-difference discretizations of (13) and (14), only the curvature term $\alpha'(s)$ requires much thought. To discretize this, write

$$\frac{d\alpha}{ds} \approx \frac{\Delta\alpha}{\Delta s} \approx \frac{\sin\Delta\alpha}{\Delta s}.$$

The sine of the turning angle $\Delta\alpha_i$ between consecutive segments $(r_i - r_{i-1}, H_i - H_{i-1})$ and $(r_{i+1} - r_i, H_{i+1} - H_i)$ of

the curve is given by the determinant of the corresponding unit vectors:

$$\sin\Delta\alpha_i = \frac{(r_i-r_{i-1})(H_{i+1}-H_i)-(r_{i+1}-r_i)(H_i-H_{i-1})}{\Delta s^2}. \tag{19}$$

This leads to the following second-order discretization of (13):

$$\frac{(r_i-r_{i-1})(H_{i+1}-H_i)-(r_{i+1}-r_i)(H_i-H_{i-1})}{\Delta s^3} + \frac{H_{i+1}-H_{i-1}}{2\Delta s\, r_i} = \mathcal{B}H_i, \quad i=1,\ldots,N-1. \tag{20}$$

The remaining equations are discretized as follows:

$$(r_{i+1}-r_i)^2+(H_{i+1}-H_i)^2=\Delta s^2, \quad i=0,\ldots,N-1, \tag{21}$$

$$r_0 = 1, \tag{22}$$

$$2\frac{H_1-H_0}{\Delta s} = \mathcal{B}(H_0+\mathcal{W}), \tag{23}$$

$$r_N = \mathcal{A}, \quad \text{and} \tag{24}$$

$$H_N = H_{N-1}. \tag{25}$$

Eqs. (20)–(25) comprise a nonlinear system of $2N+3$ equations in $2N+3$ unknowns. Although this is a two-point boundary-value problem, it cannot be solved by the shooting method because the associated initial-value-problem is *extremely* sensitive to the initial conditions. We must therefore solve the nonlinear system directly.

A natural choice is Newton's method. Using a direct solver for the block tridiagonal system which arises at each iteration, we obtain a scheme which works very efficiently for values of $\mathcal{B}$ and $\mathcal{W}$ for which the solution is unique; when there are multiple solutions, however, this scheme tends to be slightly unstable if the initial guess is not good enough, in part because the subinterval lengths are *globally* constrained to all be equal. We can stabilize it somewhat by replacing this global constraint by the $N-1$ *local* constraints

$$\Delta s_{i-1,i} = \Delta s_{i,i+1}, \quad i=1,\ldots,N-1,$$

where the N subinterval lengths

$$\Delta s_{0,1}, \Delta s_{1,2}, \ldots, \Delta s_{N-1,N},$$

are now *independent* unknowns, which can adjust themselves *separately* as the Newton iterations proceed toward convergence. The modified scheme is

$$2\frac{(r_i-r_{i-1})(H_{i+1}-H_i)-(r_{i+1}-r_i)(H_i-H_{i-1})}{\Delta s_{i-1,i}\Delta s_{i,i+1}(\Delta s_{i-1,i}+\Delta s_{i,i+1})} + \frac{\Delta s_{i-1,i}^2(H_{i+1}-H_i)+\Delta s_{i,i+1}^2(H_i-H_{i-1})}{\Delta s_{i-1,i}\Delta s_{i,i+1}(\Delta s_{i-1,i}+\Delta s_{i,i+1})r_i} = \mathcal{B}H_i, \quad i=1,\ldots,N-1, \tag{26}$$

$$(r_{i+1}-r_i)^2+(H_{i+1}-H_i)^2=\Delta s_{i,i+1}^2, \quad i=0,\ldots,N-1, \tag{27}$$

$$\Delta s_{i,i+1} = \Delta s_{i-1,i}, \quad i=1,\ldots,N-1, \tag{28}$$

$$r_0 = 1, \tag{29}$$

$$2\frac{H_1-H_0}{\Delta s_{0,1}} = \mathcal{B}(H_0+\mathcal{W}), \tag{30}$$

$$r_N = \mathcal{A}, \quad \text{and} \tag{31}$$

$$H_N = H_{N-1}. \tag{32}$$

4.1. Discussion

The above scheme works extremely well when the initial guess is sufficiently good. For small values of $\mathcal{W}$ we can simply use $r_i = s_i$, $H_i = 0$ as the initial guess. For larger values of $\mathcal{W}$, however, this is not good enough for convergence. A crude but effective "marching" procedure is to solve the problem (for a given value of $\mathcal{B}$) for a sequence of values of $\mathcal{W}$ beginning with 0, and use the each converged solution as the initial guess for the next computation.

Since our principal objective is to determine maximum disk weight that can be supported (and the associated value of α_0), there is another consideration. Since we expect that there will be no solution if $\mathcal{W}$ is too large, the scheme should begin to fail when $\mathcal{W}$ gets too close to its maximum value. To determine this maximum, therefore, we must replace the vertical force balance equation (30) by another condition at $s=0$, and compute $\mathcal{W}$ as an output variable. The most natural candidates are the Dirichlet condition

$$H_0 = \text{given} \tag{33}$$

and the Neumann condition

$$\alpha_0 = \text{given}.$$

The latter can be expressed in terms of the r_is and H_is as

$$r_1 - r_0 = (\cos\alpha_0)\Delta s_{0,1}, \quad H_1 - H_0 = (\sin\alpha_0)\Delta s_{0,1}. \tag{34}$$

Since this is two equations rather than one, we compensate by dropping Eq. (27) for $i=0$ (which is an immediate consequence of (34) anyway).

With either (33) or (34) the solution is nonunique for certain values of the free parameter (H_0 or α_0, respectively). The decision as to which to use therefore depends on how close we are to a turning point on the solution curve; near such a point, two solutions are very close together, and the scheme will be unstable unless the chosen boundary condition at $s=0$ ((33) or (34)) is associated with the parameter (H_0 or α_0) which best *distinguishes* the two solutions. By switching back and forth between the Dirichlet and Neumann conditions, we can trace out the entire solution curve by using the marching procedure alluded to above.

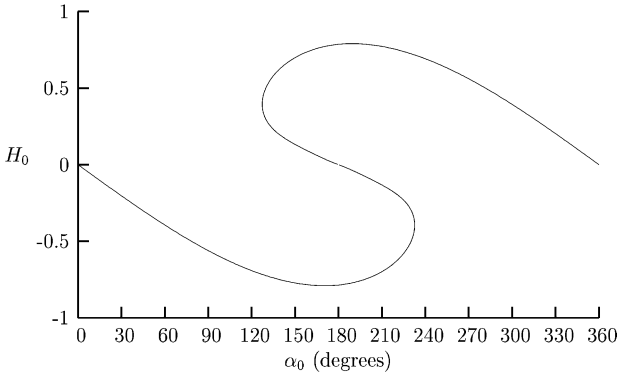

Fig. 2. Solution curve for $\mathcal{A} = 10$ and $\mathcal{B} = 4.4$.

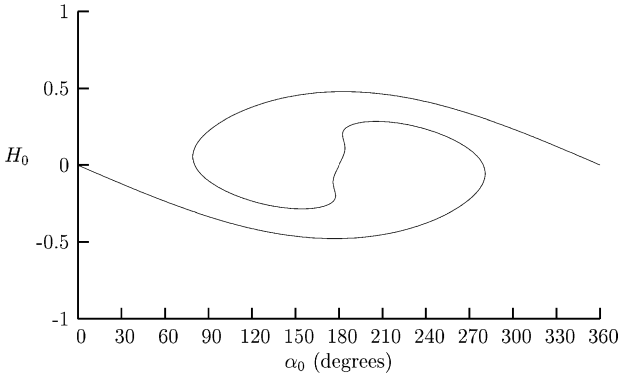

Fig. 3. Solution curve for $\mathcal{A} = 10$ and $\mathcal{B} = 14.4$.

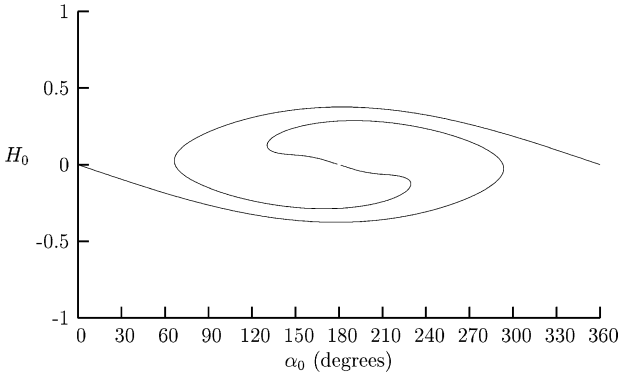

Fig. 4. Solution curve for $\mathcal{A} = 10$ and $\mathcal{B} = 24.4$.

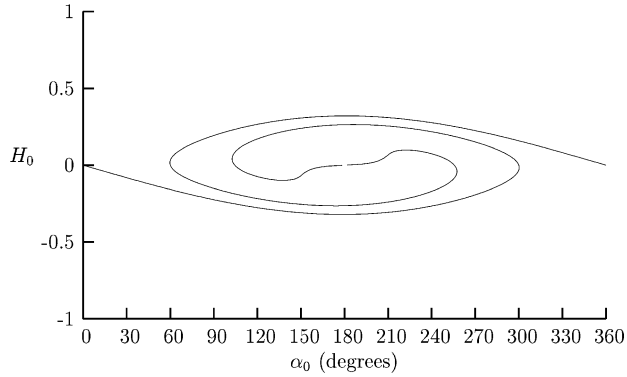

Fig. 5. Solution curve for $\mathcal{A} = 10$ and $\mathcal{B} = 34.4$.

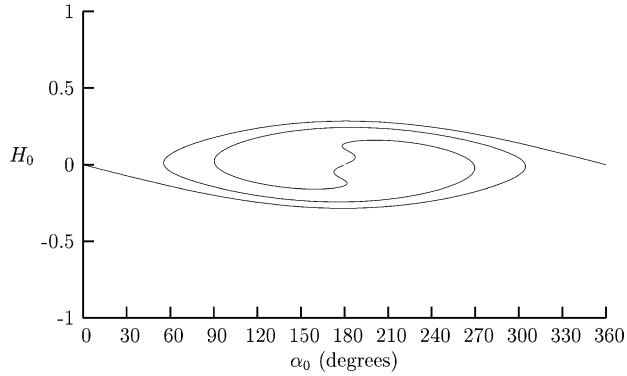

Fig. 6. Solution curve for $\mathcal{A} = 10$ and $\mathcal{B} = 44.4$.

5. Results

The solution curves for $\mathcal{A} = 10$ and $\mathcal{B} = 4.4$, 14.4, 24.4, 34.4, and 44.4 are shown in Figs. 2–6. Only the lowermost branch of each curve, for α_0 between 0° and 180°, is of physical interest. (Indeed, the remainder of the curve includes pairs (α_0, H_0) for which the corresponding surface shape has unphysical self-intersections.)

Each curve is symmetric about the point $\alpha_0 = 180°$, $H_0 = 0$. The "lower" half of each was obtained by calculating the solution for a sequence of pairs (α_0, H_0)—593, 761, 758, 832, and 879 pairs, respectively—and switching back and forth between the Neumann and Dirichlet inner boundary condition as necessary, in the manner described above. The "upper" half of each curve was obtained by reflection. All calculations were performed using $N = 131\,072$. (When $\alpha_0 = 180°$ and $H_0 = 0$, the solution of the initial-value problem is $(r(s), H(s)) = (1 - s, 0)$, $0 \leqslant s < 1$. Since $r(s)$ never reaches $\mathcal{A}$, there is no corresponding solution of either the Dirichlet or the Neumann boundary-value problems. Technically, therefore, the solution curve does *not* include the point $\alpha_0 = 180°$, $H_0 = 0$.) From these curves it is clear that the Neumann problem has multiple solutions if α_0 is in a certain interval symmetric about 180°. (The Dirichlet problem *always* has multiple solutions.)

Fig. 7 shows how $\mathcal{W}$ varies with α_0 along the lowermost branches of the computed solution curves. For each value of $\mathcal{B}$, $\mathcal{W}$ reaches a maximum and decreases thereafter, in accord with the qualitative argument of Section 2. Recall that in that argument we assumed that when $\mathcal{W}$ is maximum, H_0 is decreasing at a rate of order 1. The numerically computed solution curves show that this is indeed the case. The maximum values of $\mathcal{W}$ and the associated values of α_0 are reported in Table 1.

To check for convergence with respect to mesh refinement, we performed a parallel series of calculations using $N = 65\,536$; the maximum values of $\mathcal{W}$ were the same as those reported in Table 1 to the accuracy reported. And to check that $\mathcal{A} = 10$ is large enough to qualify as "∞," we performed another parallel series of calculations using $\mathcal{A} = 20$

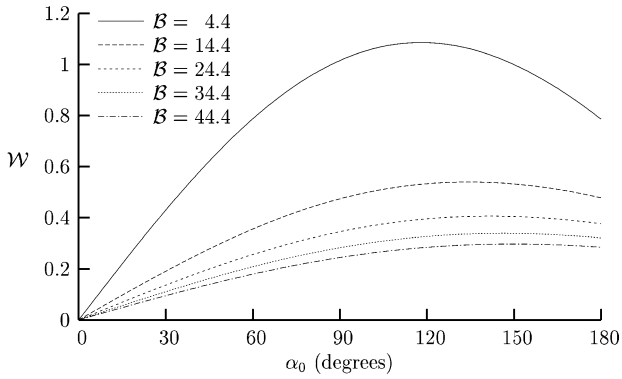

Fig. 7. $\mathcal{W}$ versus α_0 along lowermost branches of the calculated solution curves ($\mathcal{A} = 10$, $N = 131\,072$).

Table 1
The maximum values of $\mathcal{W}$ and the associated values of α_0 for the calculated solution curves ($\mathcal{A} = 10$, $N = 131072$)

$\mathcal{B}$	α_0	$\mathcal{W}$
4.4	118°	1.0857
14.4	134°	0.54015
24.4	142°	0.40618
34.4	146°	0.33923
44.4	150°	0.29736

(and $N = 131\,072$); the maximum values of $\mathcal{W}$ differed from those reported in Table 1 by only 2 in the fifth decimal place.

In actual experiments for $\mathcal{B} = 34.4$ conducted in the laboratory of the second author, the contact angle α_0 does not go much beyond about 80° before the disk breaks free and falls to the bottom of the container. The reason for this is not clear. Perhaps the contact angle α_0 locally exceeds the advancing contact angle because of small fluctuations in either (1) the downward force applied to the disk to simulate increasing buoyant weight, or (2) the orientation of the disk. This would lead to wetting of the upper surface of the disk, allowing it to sink. Another possibility is that the surface shape itself is somewhat unstable when $\alpha_0 > 90°$. It is also conceivable that a more refined experimental technique might allow these large contact angles to be achieved.

6. Summary

A simple mathematical argument shows that as the weight of a floating disk is gradually increased, the maximum contact angle at its sharp rim which is attained before the disk sinks is greater than 90°. This conclusion is supported by numerical results.

Acknowledgments

This work was supported by the National Science Foundation and the DOE (Engineering Research Program of the Department of Basic Engineering Sciences).

References

[1] H.M. Princen, The equilibrium shape of interfaces, drops, and bubbles. Rigid and deformable particles at interfaces, in: E. Matijević (Ed.), Surface and Colloid Science, vol. 2, Wiley–Interscience, New York, 1969, pp. 1–84.